Manufacturing Technologies and Applications
MATECA

Tribological Performance of Tetrahedral Amorphous Carbon (ta-C) Coatings on Plasma-Nitrided X153CrMoV12 Cold Work Tool Steel

Selim Unal[1,*], Cihangir Tevfik Sezgin[2]

[1]*Department of Metallurgical and Materials Engineering, Faculty of Engineering and Architecture, Kastamonu University, Kastamonu, Türkiye*
[2]*Department of Machinery and Metal Technologies, Kastamonu Vocational School, Kastamonu University, Kastamonu, Türkiye*

ABSTRACT

Diamond-like carbon (DLC) coatings, specifically tetrahedral amorphous carbon (ta-C), provide hard, low-friction carbon films suitable for tribological applications in demanding industrial environments. In this study, we investigated diamond-like carbon (ta-C) deposited by PVD arc technology (Ionbond Tetrabond), its quality, and applicability on tool steels, X153CrMoV12. Three different surface treatments were applied: plasma nitriding (535 °C, 9 h), DLC coating, and duplex plasma nitriding combined with DLC coating. The DLCs were characterized using characterization techniques, such as Raman, XPS, SEM, and XRD. XPS analysis reveals sp^3 fractions of approximately 60% (DLC-only coating) and 62% (duplex nitrided + DLC coating) which confirm the high quality of the deposited ta-C films. Wear tests were conducted under loads of 10 N and 20 N, with a speed of 0.04 m/s and a distance of 100 m. Low coating thickness (~400 nm) limited load-carrying capacity, leading to premature wear and substrate exposure, as well as increased friction under continuous loads. Compared to non-coated samples, ta-C coating exhibits improved adhesion resistance to delamination if deposited on a nitrided substrate. The duplex nitrided and DLC-coated configuration achieved the most significant reduction in wear track width of up to 78% compared to the uncoated baseline, establishing it as the optimal surface treatment strategy for industrial cold-forming applications. The coefficient of friction (CoF) for the duplex-treated sample remained the lowest throughout testing, confirming its superior tribological performance. This research paves the way to improvements in tool steels and coating technology of diamond-like carbon.
Keywords: *Diamond-like carbon, Tetrahedral amorphous carbon, Cold work tool steels, Wear, Plasma nitriding, Surface characterization*

Plazma Nitrürlenmiş X153CrMoV12 Soğuk İş Takım Çeliği Üzerine Tetrahedral Amorf Karbon (ta-C) Kaplamalarının Tribolojik Performansı

ÖZET

Elmas benzeri karbon (DLC) kaplamalar, tetrahedral amorf karbon (ta-C) gibi, zorlu endüstriyel ortamlardaki tribolojik uygulamalar için uygun, sert ve düşük sürtünmeli karbon filmler sağlamaktadır. Bu çalışmada, PVD ark teknolojisiyle (Ionbond Tetrabond) biriktirilmiş elmas benzeri karbon (ta-C), kalitesi ve X153CrMoV12 takım çeliklerine uygulanabilirliği araştırılmıştır. Plazma nitrürleme (535°C, 9 saat), DLC kaplama ve dupleks plazma nitrürleme ile DLC kaplama olmak üzere üç farklı yüzey işlemi uygulanmıştır. Bu işlemlerin kimyasal ve fiziksel özellikleri Raman, XPS, SEM ve XRD gibi karakterizasyon teknikleri kullanılarak karşılaştırılmıştır. XPS analizi, yalnızca DLC kaplama için yaklaşık %60, dupleks nitrürleme + DLC kaplama için %62 oranında sp^3 fraksiyon değerlerini ortaya koymuş; bu sonuçlar yüksek kaliteli ta-C filmlerini doğrulamaktadır. Aşınma testleri, 10 N ve 20 N yükler altında, 0,04 m/s hız ve 100 m mesafede gerçekleştirilmiştir. Düşük kaplama kalınlığı (~400 nm), yük taşıma kapasitesini sınırlamış; erken aşınmaya ve alt tabakanın açığa çıkmasına yol açmış, aynı zamanda sürekli yükler altında artan sürtünmeye neden olmuştur. Kaplanmamış numunelerle karşılaştırıldığında, ta-C kaplamanın nitrürlü bir alt tabaka üzerine biriktirildiğinde delaminasyona karşı gelişmiş yapışma direnci sergilediği görülmektedir. Dupleks nitrürleme ve DLC kaplama konfigürasyonu, kaplanmamış referans numuneye kıyasla aşınma izi genişliğinde %78'e varan en belirgin azalmayı sağlamış ve endüstriyel soğuk şekillendirme uygulamaları için en uygun yüzey işleme stratejisi olarak öne çıkmıştır. Dupleks işlem uygulanmış numunenin sürtünme katsayısı (CoF), test boyunca en düşük değerde kalmış; bu durum söz konusu numunenin üstün tribolojik performansını doğrulamaktadır. Bu araştırma, takım çeliklerinde ve elmas benzeri karbon kaplama teknolojisindeki ilerlemelere zemin hazırlamaktadır.
***Anahtar Kelimeler**: Elmas benzeri karbon, Tetrahedral amorf karbon, Soğuk iş takım çelikleri, Aşınma, plazma nitrürleme, Yüzey karakterizasyonu*

*Corresponding author, e-mail: sunal@kastamonu.edu.tr

Received 18.03.2026; Accepted 04.05.2026
https://doi.org/10.52795/mateca.1912748
To cite this article: S. Unal, C.T. Sezgin, Tribological Performance of Tetrahedral Amorphous Carbon (ta-C) Coatings on Plasma-Nitrided X153CrMoV12 Cold Work Tool Steel, Manufacturing Technologies and Applications 7(2)(2026) 61-78.

1. INTRODUCTION

Cold work tool steels play a significant role in drilling, ensuring operational efficiency and durability. Coated and uncoated drill bits demonstrate different wear characteristics [1,2]. High-speed steels exhibit considerable flank wear, reducing tool life and surface quality [3,4]. Drill bit quality and durability can be improved with coatings, which reduce friction at the cutting edge, enhancing hardness and thermal stability, and prolonging tool life. To achieve optimal performance in tool steels, diamond-like carbon (DLC) coatings are highly attractive due to their high hardness, low friction, and excellent wear resistance [5,6]. DLC coatings include a mixture of sp^2 (graphitic) and sp^3 (diamond-like) hybridized carbon, configurations in which sp^3 bonds impart hardness and wear resistance closer to that of natural diamond [7]. Optimizing the surface microstructure of the steel substrate through nitriding or micro-texturing can improve adhesion and coating durability [8,9]. The formation of interlayers with Mo-W or CrN can enhance the bonding of DLC coatings, thereby improving coating stability [10]. DLC coatings reduce the environmental impact of machining processes, energy requirements during drilling, and the need for cutting fluids, providing sustainable operations [11]. The integration of DLC films onto tool steel substrates offers a pathway to extend tool life and reduce maintenance costs substantially [12].

Tetrahedral diamond-like carbon (ta-C) is a form of amorphous carbon with a high fraction of sp^3 (tetrahedral) bonding. It can be achieved through deposition techniques such as plasma-arc, ion beam, and pulsed laser deposition. The resulting materials exhibit up to 86% or more tetrahedral bonding, depending on the synthesis conditions, and properties approaching similar hardness, stiffness, and transparency of diamond itself, along with an optimized bonding network, assisting in minimizing wear and fatigue [13–17]. Ta-C films exhibit hardness around 80 GPa and a Young's modulus of 700 Gpa [18,19]. In harsh environments, ta-C coatings exhibit robust thermal stability and chemical inertness [19,20]. Low friction and resistance to adhesive and abrasive wear make ta-C an ideal candidate for microelectromechanical systems (MEMS) and protection of moving parts [21]. The corrosion and biofouling resistance of ta-C supports its use in biomedical devices, utilized in antibacterial applications [22,23]. The high sp^3 content in ta-C leads to strong mechanical, optical, and corrosion-resistant properties, establishing protective coatings and potential electronic applications [14,24].

Ta-C deposited by PVD arc technology (Ionbond Tetrabond) is a coating process via physical vapor deposition (PVD) used for turbine blades, drilling equipment, and other components in aerospace and industrial applications. The PVD arc technology utilizes an arc that can undergo dynamic movement to prevent localized temperature increases and subsequent thermal resistance changes, ensuring uniform erosion of the cathode material and reduced macroparticles and defects in the arc-PVD processes [25]. The deposition occurs below 150°C, avoiding heat-related changes in the substrates. The film thickness can range from 0.4 to 1.5 µm.

In this study, we coated ta-C on tool steels. First, the tool steel was plasma-nitrided to form a hardened subsurface layer, thereby enhancing its load-bearing capacity and adhesion. The nitrided and non-nitrided substrates were coated with ta-C supplied by Ionbond. The quality of the ta-C coatings was evaluated using characterization techniques, including Raman spectroscopy, X-ray diffraction (XRD), X-ray photoelectron spectroscopy (XPS), scanning electron microscopy (SEM), and energy-dispersive X-ray spectroscopy (EDX). The coating thickness was determined by edge imaging using SEM. Tribological properties were investigated by generating wear tracks under 10 N and 20 N in reciprocating tests. Subsequently, the width and composition of the tracks were assessed using SEM and EDX, respectively. The duplex nitrided + ta-C configuration exhibits the best performance, characterized by reduced wear track widths and minimal delamination. Load-dependent oxidative behavior is revealed by EDX analysis. These surface treatments hold promise for industrial applications in cold-forming tools, extending their operational lifespan.

2. MATERIAL AND METHOD

A cold-work tool steel, DIN 1.2379 (X153CrMoV12), was provided by Sağlam Metal Company. The steels had a long, cylindrical shape with a diameter of 2 cm. They consist of C (1.55%), Cr (12%), Mo (0.8%), V (0.9%), and Fe. DIN 1.2379, X153CrMoV12, belongs to the ledeburitic cold work tool steel group with 12% chromium content. The undissolved carbon forms metal carbides, which give the steel high wear resistance and toughness, making it suitable for applications requiring crushing, cutting, and wear resistance. The tool steels were cut to a thickness of 1 cm for analysis. In addition to the base substrate, three different samples were prepared: bare nitrided, DLC-coated, and duplex nitrided and DLC-coated.

Table 1. Description of the analyzed samples.

Sample Number	Description
1	Base Material
2	Nitrided
3	DLC Coated
4	Nitrided + DLC Coated

In Table 1, sample 1 represents the uncoated base material, while sample 2 underwent plasma nitriding at 535°C for 9 hours before controlled cooling. DLC deposition was performed using PVD arc technology (Ionbond Tetrabond) to ensure commercial reproducibility. The manufacturer's standard recipe was used for tool steel to prevent localized temperature increases and defects. Prior to DLC application, a chromium layer was deposited to facilitate adhesion. A synergistic effect was sought by applying a plasma nitriding pre-treatment before DLC deposition on the final substrate, enabling a comprehensive comparison between the duplex system and individual coatings. Wear tests were conducted under loads of 10 N and 20 N, with a speed of 0.04 m/s and a distance of 100 m. Three tests were performed for each load and distance, and the average wear volumes were calculated. The wear tests were carried out using a 4D-ECN brand linear (reciprocating) wear testing device. A 6 mm diameter Al2O3 ball was used as the counterbody. The wear volumes were calculated according to the ASTM G99 standard. According to this standard, the formula used to determine the wear volume is as follows:

$$h = R - \sqrt{R^2 - \left(\frac{d}{2}\right)^2} \tag{1}$$

$$V = \frac{h\pi}{2}\left(3\left(\frac{d}{2}\right)^2 + \frac{h^2}{3}\right) \tag{2}$$

R is the radius of the ball, d is the diameter of the wear trace, h is the estimated wear depth derived from the spherical geometry (radius difference), and V is the estimated wear volume [26].

Although ASTM G99 is designed for pin-on-disk tests, the wear volume in the reciprocating ball-on-flat configuration was estimated using the spherical cap geometry. The wear scar diameter was measured using optical microscopy, and the wear volume was calculated from this parameter based on the spherical geometry equations. While profilometry offers direct volume measurement, this geometric calculation is widely adopted in the literature to provide a consistent relative comparison of wear resistance between the sample variants [27,28].

Following the tests, energy-dispersive X-ray spectroscopy (EDX) and scanning electron microscopy (SEM) analyses were conducted on the wear tracks and cross-sectional views of the coatings. Initially, the thicknesses of the layers were determined from the cross-sectional images. Subsequently, EDX analyses were performed to observe elemental changes in the wear tracks. The wear damage within the wear tracks was examined and evaluated.

The chemical composition and quality of the DLC coating were examined using scanning electron microscopy (SEM) and energy-dispersive X-ray spectroscopy (EDX) (FEI Quanta FEG 250). An X-ray diffractometer (Bruker D8 Advance XRD) at 40 kV voltage under Cu Kα radiation was used to analyze the ta-C structure. The phase positions were determined by scanning at an angle range of 5°<2θ<130° with a scanning speed of 1 min^{-1}. The surface chemistry and possible structural changes of the coating were analyzed using laser Raman spectroscopy. Raman peaks were obtained using a 532 nm laser (Renishaw inVia) in the wavenumber range of 100 cm^{-1} to 4000 cm^{-1}. The chemistry and elemental concentrations of the coating were determined using X-ray Photoelectron Spectroscopy (XPS, Thermo Scientific K-alpha). The ion beam energy was set to 30 eV and 150 eV, with Al K-alpha micro-focused ion sources directing ions onto the coating, resulting in a spot size of 400 µm. At least ten scans were performed for each dataset.

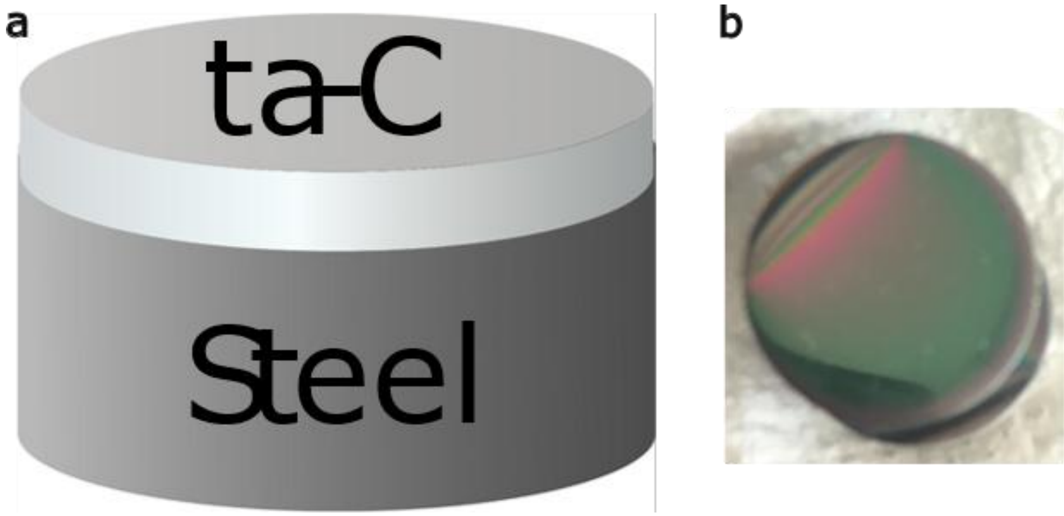

Figure 1. a) Schematic and b) image of a ta-C deposited cold work tool steel.

3. RESULTS AND DISCUSSION

3.1. Spectroscopic Characterization

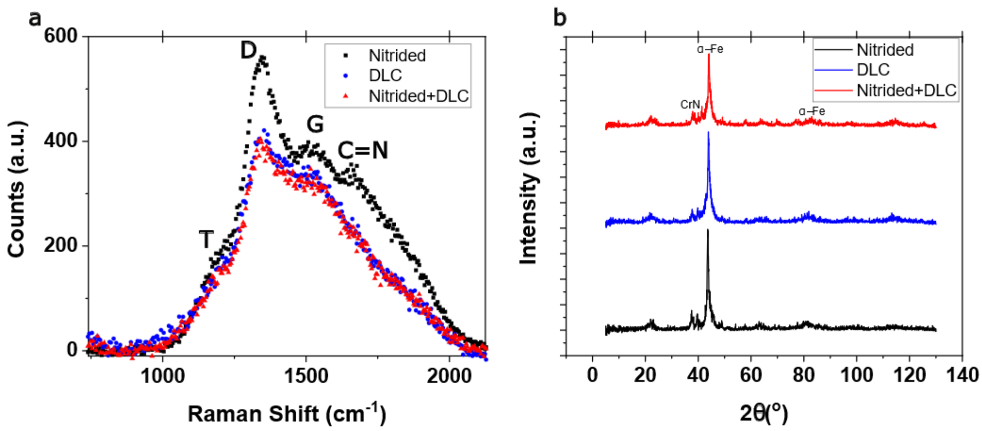

Figure 2. a) Raman and b) XRD spectra of the nitrided, DLC-coated, and both nitrided and DLC-coated cold work tool steels.

Raman spectroscopy is one of the easiest techniques to analyze the quality of carbon coatings, such as DLC. Raman scattering reveals resonant processes of carbon atoms. The Raman spectra of DLC films reveal two types of bonding: sp^3 (diamond-like) and sp^2 (graphite-like). The Raman spectra of DLC provide information about its bonding structure (Figure 2a), sp^3/sp^2 ratio, and mechanical properties. The D band, centered around 1350 cm^{-1}, represents the disorder arising from the breathing mode of sp^2 carbon atoms in aromatic rings, as observed in disordered nanocrystalline graphite [29]. The G band, located around 1550 cm^{-1}, corresponds to the graphitic bond and represents the stretching mode of sp^2 carbon atoms [30]. The T band is occasionally observed in hydrogenated DLC or ta-C at around 1100 cm^{-1}, which is associated with sp^3 carbon vibrations [31].

Table 2. I(D)/I(G) ratios for different tool steel treatments.

Tool Steel	**I(D)/I(G)**
Nitrided	1.439458
DLC	1.212845
Nitrided+DLC	1.150365

A higher I(D)/I(G) ratio indicates greater disorder and more graphitic sp^2 domains on the surface, shown in Table 2. The I(D)/I(G) ratio decreases as the DLC is deposited on the surface. The nitrided tool steel has the ratio around 1.44, resembling graphite. With the DLC coating, the ratio reduces to 1.21, indicating a higher sp^3 content in the DLC film. The nitrided layer improves adhesion of the DLC coating, allowing a denser, higher sp^3 content DLC film. The deposited DLC dominates the surface properties, potentially masking some steel and nitride-related carbon features. The high carbon content of the tool steel also diminishes the proper DLC quality interpretation. The XRD results shown in Figure 2b demonstrate that the α-Fe peak intensity decreases with the DLC coating. The surface coverage of DLC attenuates X-ray penetration into the underlying steel substrate, reducing the intensity of crystalline α-Fe peaks. This reduction enhances wear resistance.

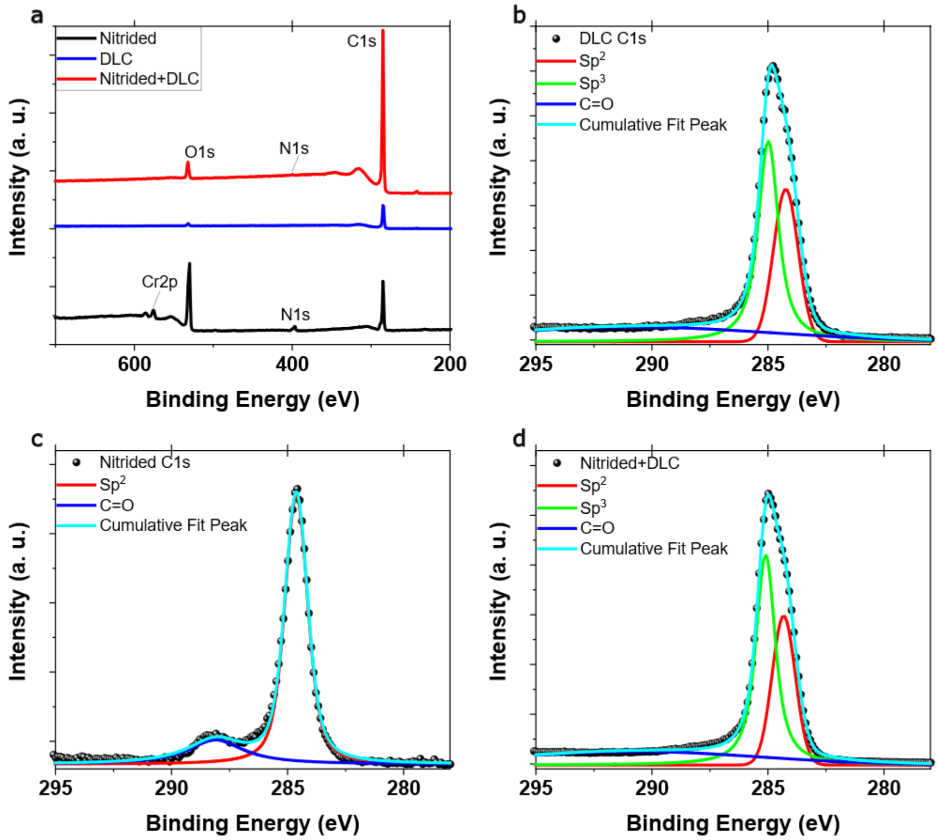

Figure 3. a) XPS spectra of tool steels. b) C1s XPS spectra of DLC-coated, c) nitrided, and d) both nitrided and DLC-coated tool steels.

Nitrided tool steels have significant surface oxygen, chromium, and carbon peaks, shown in Figure 3a. A slight nitrogen peak around 397 eV appears for the nitrided surface. Surface oxidation or oxygen contamination peak is at 532 eV. DLC coating raises the C1s peak for both nitrided and DLC-coated steels. DLC coating suppresses the surface oxygen and reduces the oxygen-to-carbon ratio. Nitrided tool steels exhibit a high level of surface oxygen due to the nitriding process, generating a slight oxidation layer [32]. A slight oxygen peak for the solely DLC-coated steel might result from the surface oxidation. The carbon-oxygen ratio is slightly higher in the nitrided+DLC coated steels than in the only DLC coated one. This is attributed to the nature of DLC coatings, which form a dense carbon network, enhancing the adherence of the DLC with increased surface roughness and mechanical anchorage from the nitrided layer [33,34]. Mechanical properties brought about by the nitriding, along with any reactive oxygen species from environmental exposure, affect the tribological characteristics of the treated steels [35].

Figure 3 shows the C1s peak around 285 eV, reflecting carbon, sp^2, and sp^3 contributions. They were investigated by Voigt function fitting as the peaks exhibit neither Gaussian nor Lorentzian due to multiple broadening mechanisms inherent to the XPS process [36]. Nitrided tool steel presents only a single sp^2 peak at 284.6 eV. A broad C=O peak also appears for all samples around 288 eV for carbonyl or carboxyl groups [36–39]. DLC coating introduces a sp^3 diamond-like bonding peak around 285 eV. The sp^2 peak shifts slightly to ~284 eV. The shift and separation are consistent with established carbon bonding state values reported in the literature [40]. The area of the two peaks indicates the sp^3/sp^2 ratios. The area of the peak ratios Asp^3/Asp^2 is 1.51 and 1.62 for only DLC-coated and nitrided and DLC-coated tool steels, respectively. To interpret these ratios, we can calculate their fraction ratios to find the percentage of sp^3 contribution using $sp^3/(sp^3+sp^2)$, which is around 60% and 62% [40]. The nitrided substrate enhances hardness, wear resistance, and adhesion by 2%, compared to the non-nitrided substrate.

Similar behavior has been observed in the Raman spectra results, as the nitrided substrate has a slightly higher sp^3/sp^2 ratio. However, the Raman spectra are difficult to fit perfectly due to their broad peaks, which may obscure several carbon features originating from the steel substrate. The steel substrate acts as a background that may influence the carbon contribution interpretation. While reducing laser power in future studies might minimize heat damage and background interference, the current spectra sufficiently indicate the presence of the mixed sp^2/sp^3 structure characteristic of DLC.

The Raman I(D)/I(G) ratio decreases from 1.44 to 1.21 from nitrided to DLC-only sample. The duplex DLC+nitrided coating shows 1.15. The decrease in I(D)/I(G) indicates a reduction in ordered sp^2 clustering and is consistent with higher sp^3 content. XPS analysis confirms this reduction as the sp3 fraction increases from approximately 60% (DLC-only) to 62% (duplex nitrided + DLC). It should be noted that XPS provides a surface-sensitive quantification using a Voigt function. The Asp^3/Asp^2 ratios are 1.51 (DLC-only) and 1.62 (duplex nitrided + DLC). The XPS results serve as a bridge to fill the analytical gap in Raman spectroscopy, confirming the increase in diamond-like bonding. Both datasets demonstrate that plasma nitriding as a pre-treatment enhances the quality of the deposited film.

3.2. Microstructural and Tribological Analysis

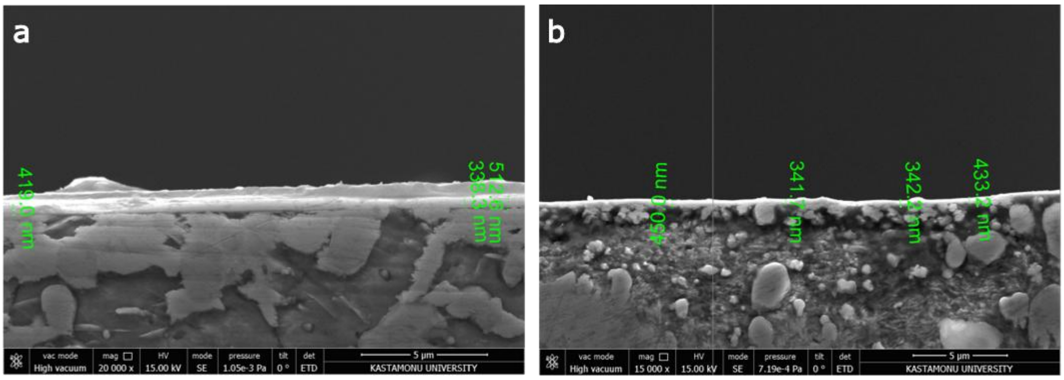

Figure 4. SEM cross-sectional images of a) DLC-coated (Sample 3), b) duplex nitrided+DLC-coated (Sample 4) cold work tool steels.

Figures 4 to 7 present the microstructural integrity, wear behavior, and elemental composition of DLC coatings applied to the cold work tool steels under varying mechanical loads. Scanning electron microscopy (SEM) and energy-dispersive X-ray spectroscopy (EDX) reveal the efficacy of surface treatments, including nitriding and DLC deposition, in enhancing wear resistance.

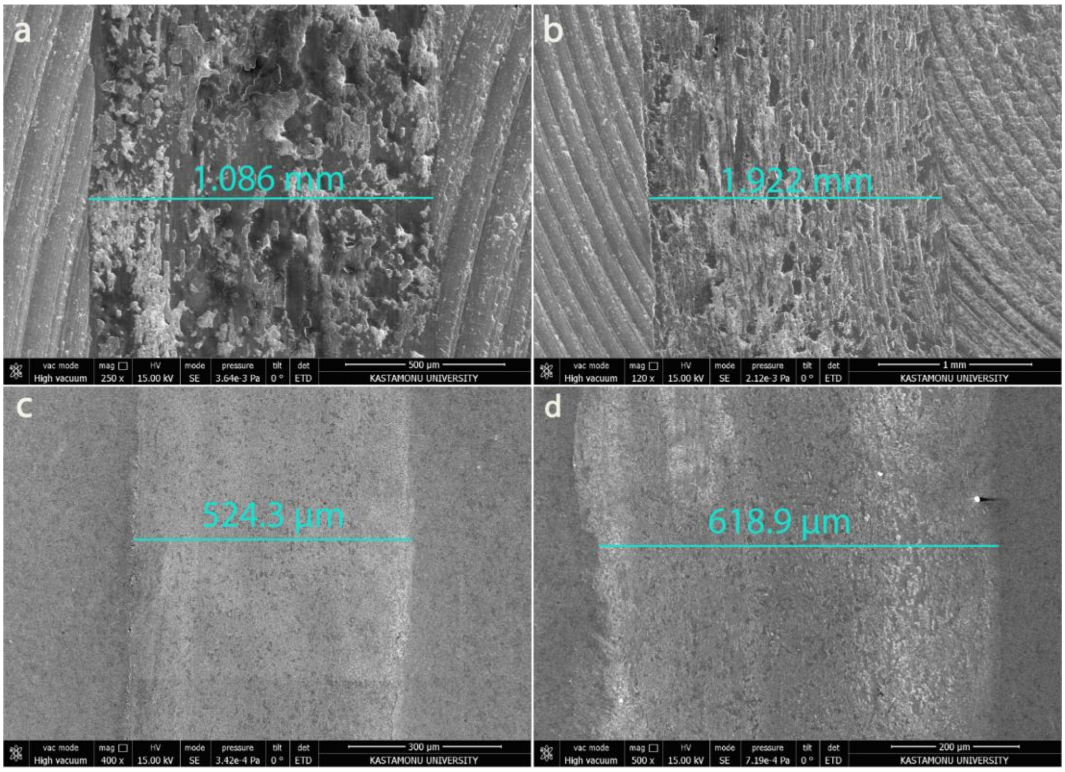

Figure 5. a) Untreated cold work tool steel 10 N and b) 20 N load. c) Nitrided tool steel under a load of 10 N and d) 20 N.

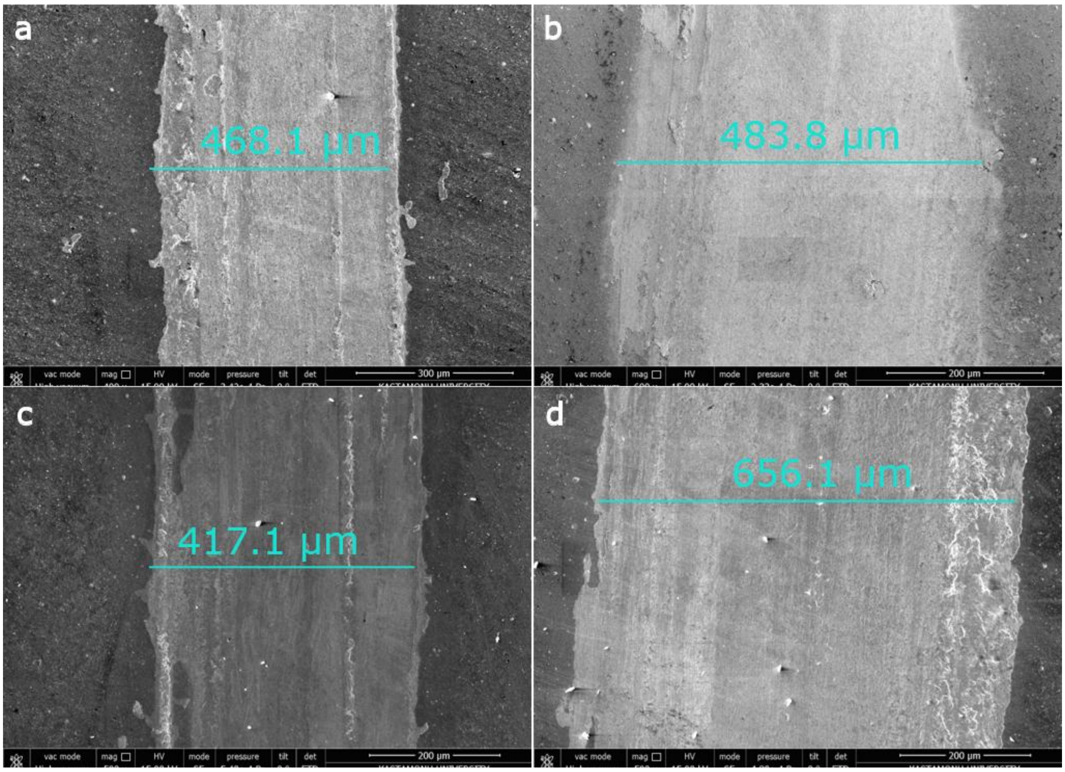

Figure 6. a) Cold work tool steel coated by DLC under the load of 10 N, b) 20 N, c) duplex nitrided and coated by DLC under the load of 10 N, and d) 20 N.

Figure 4 shows cross-sectional SEM micrographs of the coated tool steel samples, illustrating the morphology and approximate thickness of the DLC layers. The thickness was measured at three to four different locations from the cross-sectional image. The DLC-only coating measured 423.3±50.4 nm, and the nitrided+DLC sample measured 393.3±28.1 nm. These values are consistent with typical ta-C deposited by PVD arc processes [41]. Despite the surface roughness, the DLC layer appears as a dense, uniform overlayer on the top of the substrate. Due to the nitrogen-enhanced interface on the nitrided variant in Figure 4b, the nitrided DLC-coated sample exhibits a slightly more diffuse interface, indicating enhanced adhesion. The measured thickness aligns with typical DLC deposited via plasma-enhanced chemical vapor deposition (PECVD) and PVD [11,42,43].

The wear track widths from the reciprocating tribotest conducted under 10 N and 20 N are presented in Figures 5 and 6 for four sample variants: bare (Figure 5a, b), nitrided (Figure 5c, d), DLC-coated (Figure 6a, b), and nitrided + DLC-coated (Figure 6c, d). The SEM images reveal progressive improvement in wear resistance with each surface treatment.

For sample 1 (uncoated cold work tool steel), the wear tracks widths are 1.086 mm under 10 N load and 1.922 mm under 20 N load, characterized by strongly oxidized layers, indicating abrasive and oxidative wear mechanisms. The rough, fractured morphology implies severe plastic deformation and material removal, consistent with the high friction of bare tool steels under dry sliding conditions [44]. Nitriding on cold work tools forms a hardened compound layer (Fe-N phases), which shows wear widths of 0.524 mm for 10 N and 0.619 mm for 20 N load, see Figure 5c and d.

DLC-coated samples present wear widths smaller than 0.5 mm under a 10 N load. The low-friction nature of DLC reduces shear stresses, limiting wear to mild abrasive modes [45,46]. The narrowest wear marks have been seen for the duplex nitrided and DLC-coated sample. The widths are 0.417 mm and 0.656 mm under 10 N and 20 N, respectively. The 20 N load wear-marked sample has some cracking in the coating, suggesting nitriding enhances adhesion and subsurface support and allows the DLC to withstand higher loads. However, for the non-nitrided DLC sample, the marks under 20 N indicate a threshold where the thin film collapses. The high contact pressure on the softer substrate caused the coating to fracture, allowing the counterbody to reach the base material. Thus, the most stable performance is observed in the duplex sample.

Overall, the wear track width decreases by up to ≈78% with combined surface treatments and coatings compared to the uncoated baseline, indicating the load-dependent efficacy of DLC. Plasma nitriding introduces nitrogen into the steel surface, forming a Fe-N compound layer, which hardens the surface. The wear marks consistently reduce under a 10 N load with nitriding and coatings. However, some instabilities have been seen with the nitrided process. The nitriding induces compressive stresses in the surface layer due to lattice expansion, showing uniform mild abrasive wear [47].

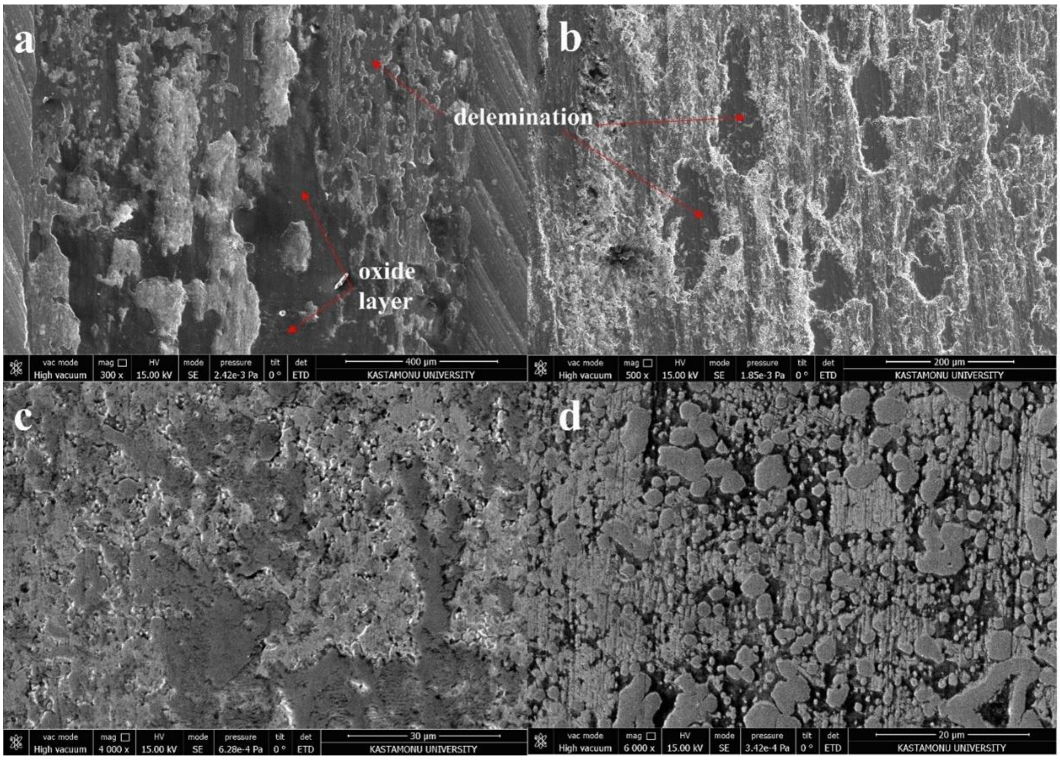

Figure 7. a) Untreated cold-worked tool steel, 10 N, and b) 20 N load. c) Nitrided tool steel under a load of 10 N and d) 20 N.

The wear damage observed in samples 1 and 2 during wear tests conducted under 10 N and 20 N loads is shown in Figure 7. In sample 1 (base steel), oxide layer and delamination formation are demonstrated during the wear test under a 10 N load. For increased load (under 20 N), the oxide layer disappears, and the number of delaminations increases. Nitrided samples do not present any delaminations. Metallic atoms are sputtered from the sample surface into the plasma, where they react with nitrogen ions near the surface and then redeposit onto the sample, forming a clustered particle morphology [48]. The pressure, temperature, and gas mixture affect the sputtering rate, which varies depending on the plasma density [49].

Figure 8 illustrates the wear damage observed on Samples 3 and 4 after wear tests conducted under loads of 10 N and 20 N. Following the 10 N wear test on the DLC-coated cold-work tool steel, an oxide layer was observed on the surface. Within this oxide layer, the formation of micro-cracks was identified. Repeated friction cycles may have caused dislocation accumulation beneath the surface, leading to the formation of micro-cracks within the oxidized shell. Due to the influence of these cracks, deep and straight grooves were observed under a 20 N load instead of a stable oxide layer. These grooves indicate abrasive wear resulting from the penetration of hard particles.

Sample 4 underwent a duplex treatment, consisting of plasma nitriding followed by DLC coating to create a dual-layer structure. Under a 10 N load, both micro-cracks and severe plastic deformation (SPD) zones were observed. SEM analysis revealed a clear deformation gradient extending from the worn surface to the bulk material, characterized by highly elongated grains in the subsurface deformation layer. The formation of these layers is attributed to dislocation motion at the atomic level.

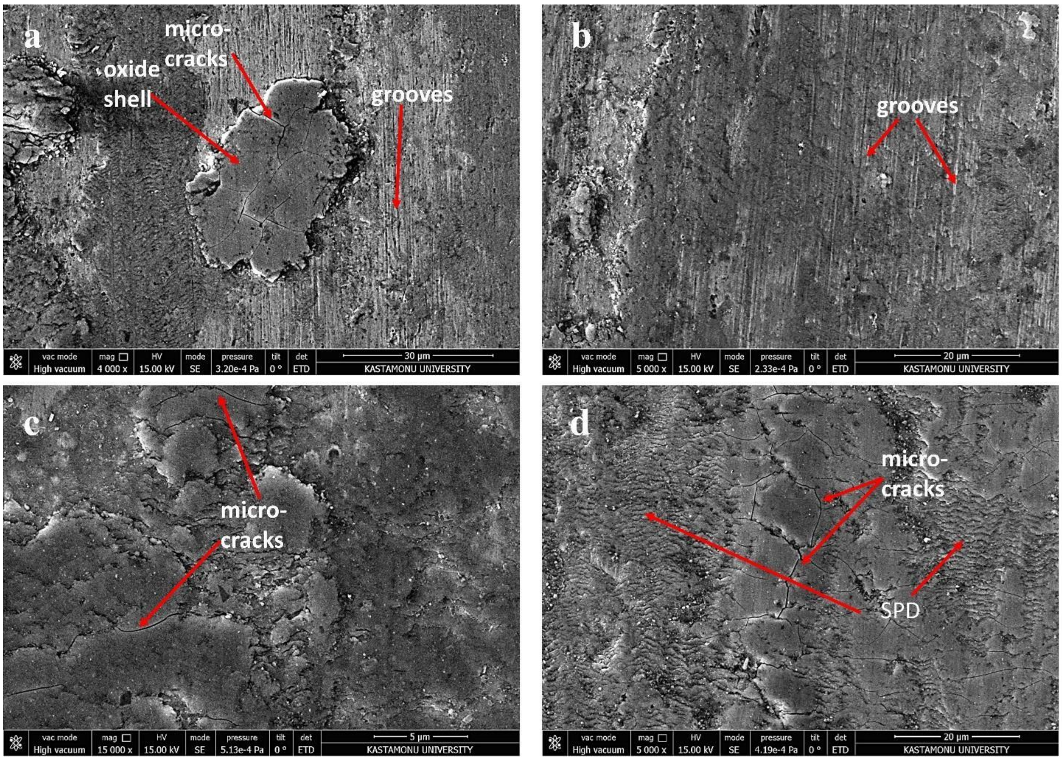

Figure 8. a) Cold work tool steel coated by DLC under the load of 10 N, b) 20 N, c) duplex nitrided and coated by DLC under the load of 10 N, and d) 20 N. (SPD; Severe Plastic Deformation).

The wear volume loss amounts calculated using formulas 1 and 2 mentioned above are shown in Table 3. The wear volume results calculated according to the ASTM G99 standard provide clear insights into the dominant wear mechanisms governing the tribological behavior of the tested samples. By correlating the quantitative wear volume data with known tribological principles, the prevailing wear mechanisms can be systematically identified and discussed for each surface condition.

Table 3. Results of the wear tests.

Sample–Force (N)	h (mm)	R (mm)	d (mm)	V (mm^3 x 10^{-3})
1–10	0.024621	6	1.086	34.212457 ± 0.93
1–20	0.077460	6	1.922	337.186663 ± 6.57
2–10	0.005730	6	0.5243	1.855558 ± 0.11
2–20	0.007985	6	0.6189	3.603476 ± 0.11
3–10	0.004567	6	0.4681	1.17887 ± 0.08

3–20	0.004878	6	0.4838	1.345199 ± 0.11
4–10	0.003626	6	0.4171	0.743082 ± 0.04
4–20	0.008975	6	0.6561	4.551526 ± 0.48

For sample 1, representing the untreated base material, the wear volume increased sharply with increasing normal load. This behavior indicates the dominance of adhesive and abrasive wear mechanisms. Under low loads, mild adhesive wear is expected due to localized junction formation between the mating surfaces. However, as the applied load increases, plastic deformation becomes more pronounced, leading to micro-ploughing and severe abrasive wear. The absence of a hardened surface layer allows the counterface asperities to penetrate deeper into the substrate, resulting in accelerated material removal.

In the case of sample 2, corresponding to the nitrided specimen, a noticeable reduction in wear volume was observed compared to the base material across all load levels. The nitrided diffusion layer effectively suppresses adhesive wear by increasing surface hardness and reducing real contact area. Abrasive wear remains the dominant mechanism; however, it occurs in a milder form due to the enhanced load-bearing capacity of the hardened surface. At higher loads, the gradual increase in wear volume suggests the onset of subsurface fatigue, although catastrophic failure is not evident.

Sample 3, representing the DLC-coated specimen, exhibited significantly lower wear volumes, particularly under low and medium loads. The dominant wear mechanism for this sample is mild abrasive wear, accompanied by a substantial suppression of adhesive interactions due to the low surface energy and low friction coefficient of the DLC coating. The high hardness of the DLC layer effectively prevents severe ploughing. Nevertheless, at higher loads, a slight increase in wear volume may indicate localized coating damage or micro-crack initiation within the coating, which is typical for hard but relatively brittle thin films.

The most favorable wear behavior was observed for Sample 4, corresponding to the duplex-treated specimen with a DLC coating deposited on a nitrided substrate. This sample consistently exhibited the lowest wear volumes over the entire load range. The dominant wear mechanism is primarily mild abrasive wear, while adhesive wear is effectively suppressed. Importantly, the nitrided layer provides strong mechanical support for the DLC coating, significantly delaying the onset of delamination wear. This synergistic effect prevents premature coating failure, which is often observed in monolayer coatings under high contact stresses.

A comparative analysis reveals that delamination wear becomes increasingly critical at higher loads, particularly for samples lacking adequate subsurface support. The untreated base material and, to a lesser extent, the solely nitrided specimen are more susceptible to subsurface crack initiation due to cyclic contact stresses. In contrast, the duplex-treated sample demonstrates enhanced resistance against crack propagation at the coating–substrate interface, thereby minimizing delamination-related material loss.

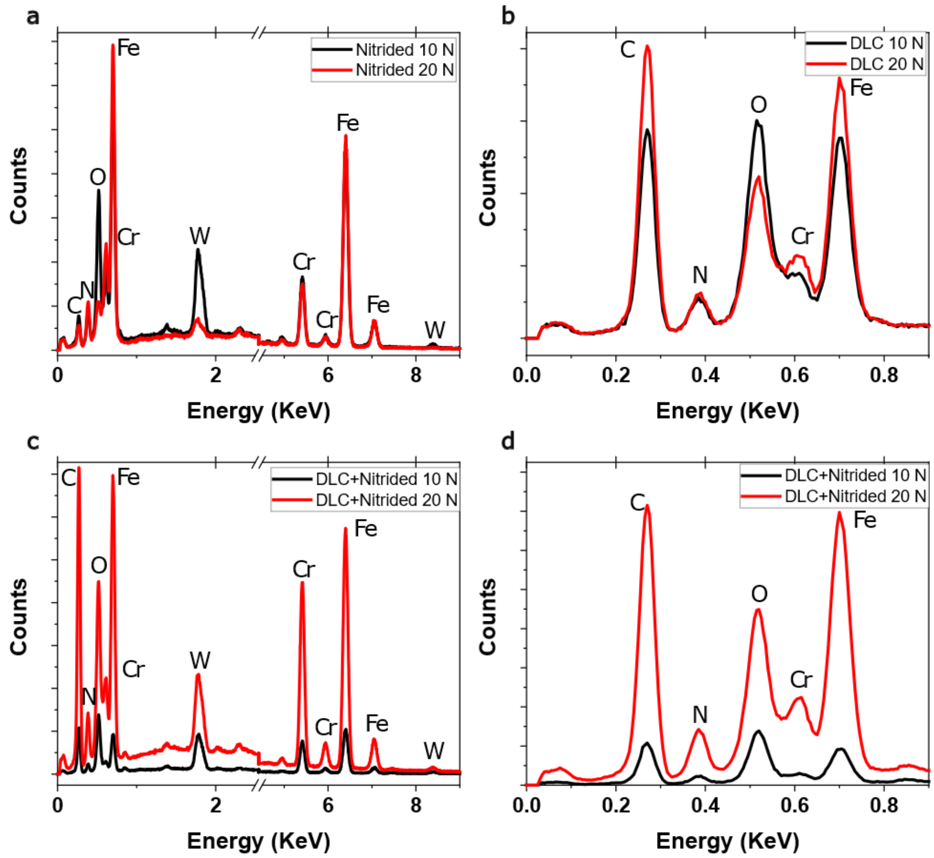

Figure 9. EDX spectra of a) nitrided, b) DLC coated (focused on between 0 to 1 keV), c) and d) DLC coated and nitrided, and focused on 0 to 1 keV cold tool steels under 10 N and 20 N loads.

The load-dependent evolution of wear mechanisms further highlights the importance of surface engineering strategies. While abrasive wear is unavoidable under sliding contact, its severity can be effectively controlled through surface hardening and advanced coatings. Adhesive wear is largely mitigated by the presence of DLC coatings, whereas delamination wear is strongly influenced by coating adhesion and substrate support.

From a critical perspective, the wear volume results confirm that single surface treatments improve wear resistance to a certain extent; however, their performance may degrade under severe loading conditions. The duplex treatment, on the other hand, provides a balanced combination of surface hardness, low friction, and structural integrity. This explains the superior and more stable wear performance observed across the entire load spectrum.

Overall, the strong agreement between the calculated wear volumes and the identified wear mechanisms enhances the reliability of the present results. The findings clearly demonstrate that the duplex nitriding + DLC coating strategy offers a robust solution for applications involving high contact loads and demanding tribological conditions. These results are therefore of direct relevance for advanced engineering components requiring long-term wear resistance.

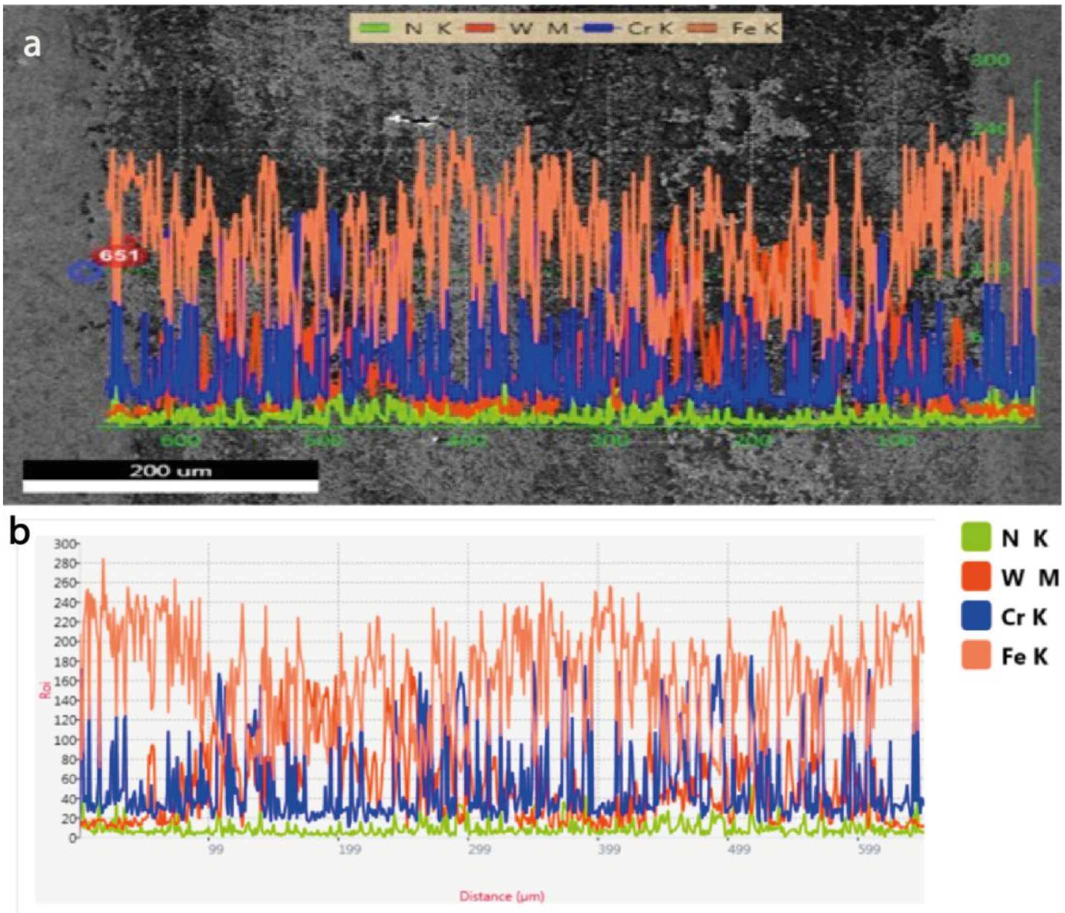

Figure 10. a) Elemental distribution graph of the wear track of sample 2, subjected to a wear test under a 10 N load, and b) its dataset. The x-axis and y-axis represent position and elemental concentration, respectively.

The wear tracks were examined using energy-dispersive X-ray spectroscopy (EDX), providing elemental mapping for chemical alterations induced by tribological interactions. Nitrided sample spectra, in Figure 9a, show a high Fe amount under both 10 N and 20 N load. Oxide and W content decrease at higher load, suggesting that oxidative wear is confined to the surface without deep substrate erosion. With the DLC coating, see Figure 9b, the carbon and iron content increases under 20 N load, confirming carbon-rich DLC presence. The 20 N load still sustains a high amount of carbon. The nitride layer adheres to the lower layers for both the nitrided and the DLC-coated samples. Possible surface oxidation is present in the surface layers as the level of oxygen decreases sharply with the load. The duplex nitrided and DLC-coated sample also shows high carbon and iron peaks, see Figure 9c and d. Under a 10 N load, the oxygen rate is still higher than the C and Fe peaks, similar to only the DLC-coated sample. The peak ratios between the DLC-coated and nitrided+DLC-coated samples demonstrate similar behavior. The formation of O and W exists on the surface layers of both nitrided and non-nitrided samples. A similar Fe ratio has been observed for all samples, indicating uniform distribution of Fe atoms.

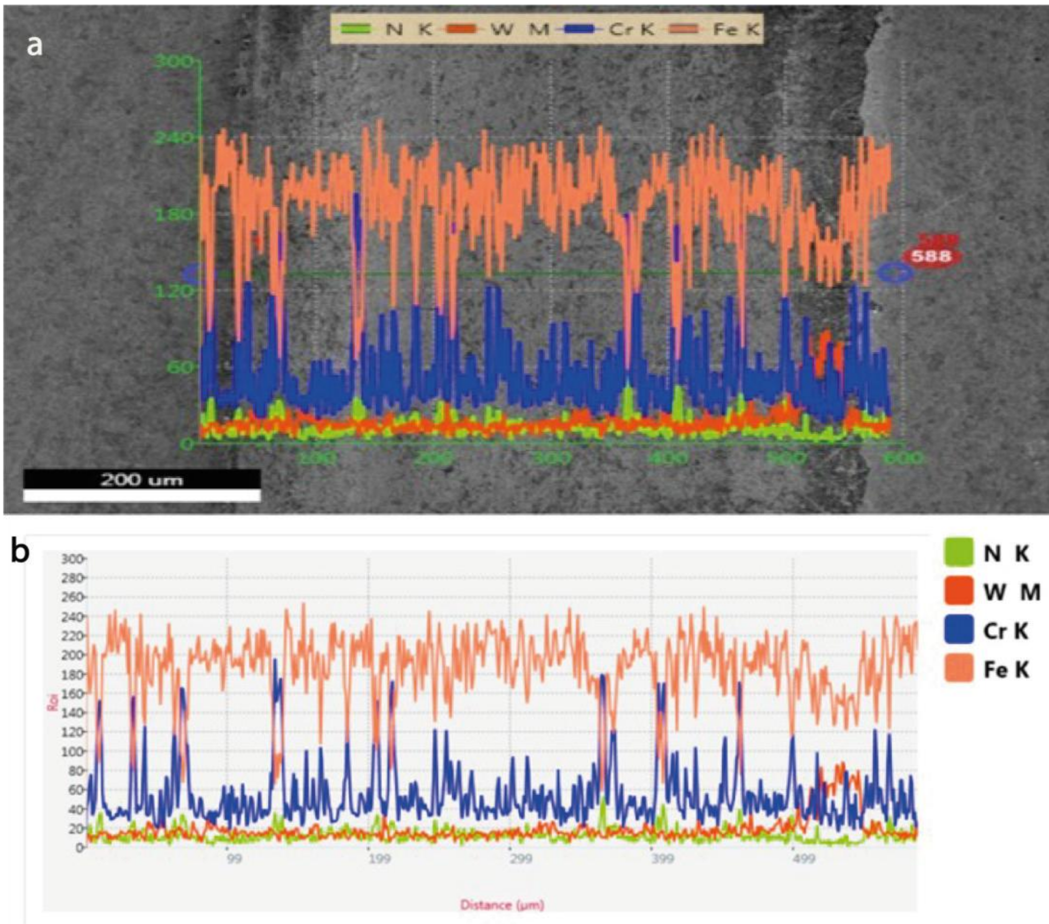

Figure 11. a) Elemental distribution graph of the wear track of sample 2, subjected to a wear test under a 20 N load, and b) its dataset. The x-axis and y-axis represent position and elemental concentration, respectively.

Figures 10a, b and 11a, b show the horizontal elemental distribution of the indentation formed as a result of the wear test of sample 2. Looking at the elemental density graphs in Figures 10b and 11b, it can be seen that nitrogen is present in lower concentrations compared to other elements. Chromium decreases at the points where iron peaks. However, when considering the relatively small peaks of nitrogen compared to other elements, it is observed that chromium also increases significantly at the same points, while iron decreases. Tungsten, on the other hand, appears to be stable. Although tungsten is also a nitride former, its thermodynamic affinity for nitrogen is lower than that of chromium. Chromium exhibits a significantly higher thermodynamic affinity for nitrogen compared to tungsten, as evidenced by its more negative Gibbs free energy of formation for nitrides (CrN) [50,51]. Therefore, chromium nitride is more stable than tungsten nitride.

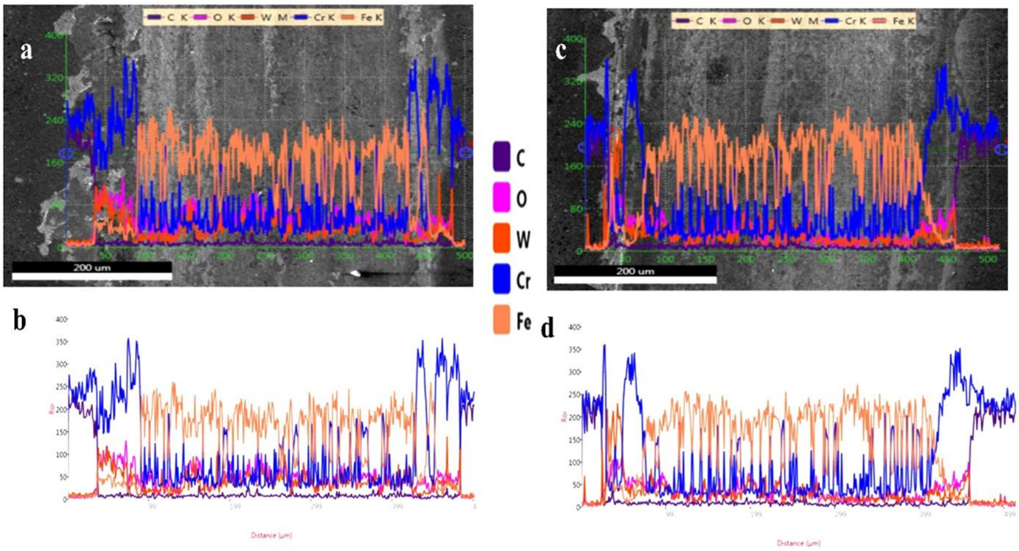

Figure 12. Elemental distribution results of the wear track formed as a result of wear tests of sample 3 under loads of a), b) 10 N and c, d) 20 N. The x-axis and y-axis represent position and elemental concentration, respectively.

Figure 12a-d show the horizontal elemental distribution of the wear track resulting from the wear test of sample 3, coated with DLC. Looking at the elemental density graph, it can be seen that the Cr and C ratios are high in areas without wear and near the edges of the wear track. The high Cr ratio is due not to the amount of Cr in the base material, but rather to the pre-chromium plating applied during DLC coating to strengthen the bond between the base material and carbon. Although a dramatic decrease in Cr and especially C is observed in the wear track, the iron ratio is seen to increase rapidly. In fact, as can be seen in Figure 4, the DLC layer thickness is quite low (approximately 400 nm). Therefore, despite the high sp^3 quality of the film, the thin DLC coating was destroyed during the wear test under 20 N load, and the alumina ball (counterbody) reached the base material. In the gray areas, it is observed that carbon is absent, but chromium is present.

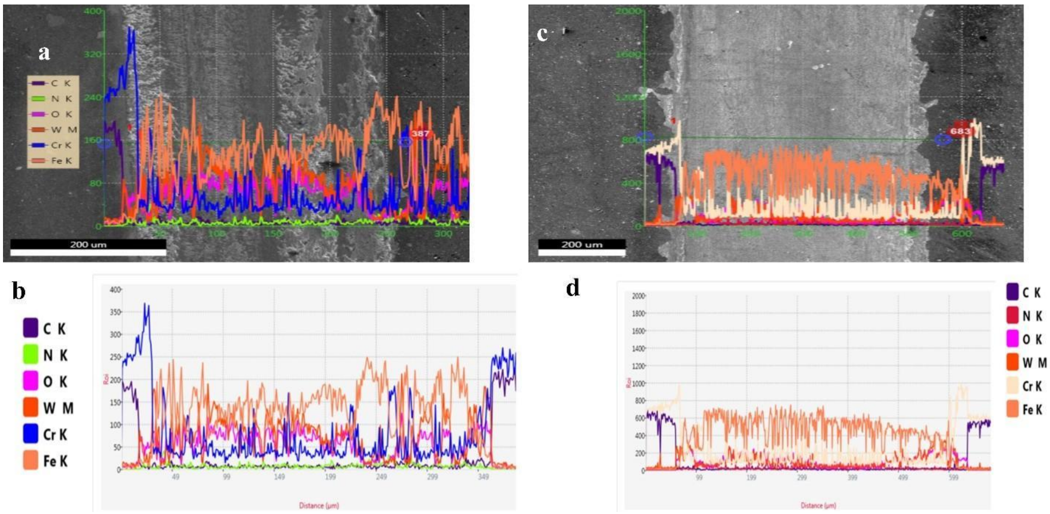

Figure 13. Elemental distribution results of the wear track formed as a result of wear tests of sample 4 under loads of a), b) 10 N and c, d) 20 N. The x-axis and y-axis represent position and elemental concentration, respectively.

Figure 13 illustrates the lateral elemental distribution within the wear track of Sample 4, which was coated with a DLC and plasma-nitrided duplex layer after the wear test. According to the elemental intensity profiles, high concentrations of Cr and C were observed in the unworn areas and regions near the edges of the wear track, consistent with Figure 12. While a significant depletion in Cr and particularly C levels was observed within the wear track, a rapid increase in Fe content was detected. Conversely, the nitrogen content remained relatively stable, albeit at low levels. These observations indicate that the counterbody (abrasive ball) wore through the tetrahedrally bonded DLC (ta-C) layer during the test; however, the underlying nitrided layer was not completely removed (Figures 13a, b). In contrast, when the load reached 20 N, the nitrogen concentration became almost negligible. This indicates that the higher load caused the nitrided layer to be completely worn away (Figure 13c, d).

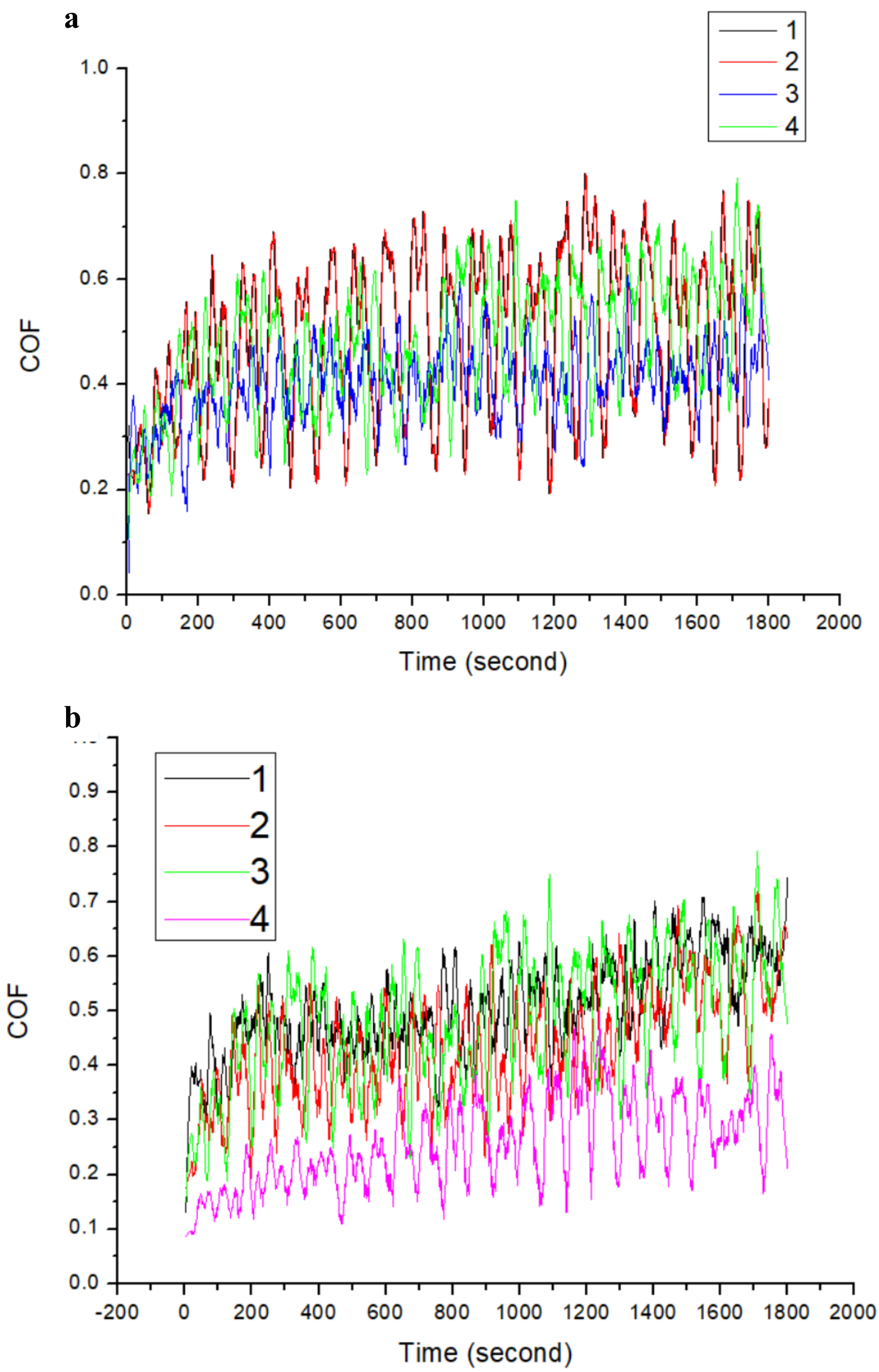

Figure 14. CoF graphs obtained from wear tests applied to samples under loads of (a) 10 N and (b) 20 N. 1, 2, 3, 4 represent the Base Material, Nitrided, DLC Coated, and Nitrided + DLC Coated samples, respectively.

Figure 14 shows the CoF graphs obtained from wear tests applied to samples under loads of 10 N and 20 N, respectively. As can be seen in Figure 14a and b, all four samples initially exhibit low CoF values; however, as the wear test progresses, deep valleys and high peaks begin to appear. In sample 1 (Base Material), which has no coating, surface fracture occurs; as a result, increased CoF values are observed due to interactions between the counterbody and these surface irregularities. For the coated surfaces, although the initial CoF values are low, especially in Sample 3 (DLC-coated) and Sample 4 (duplex nitrided + DLC-coated), pronounced deep valleys and high peaks are observed. This behavior can be attributed to the very thin coating thickness.

4. CONCLUSIONS

Tailoring the surface of cold tool steels can boost performance for use in industry. Three different surface treatments were applied to DIN 1.2379 (X153CrMoV12) tool steels, which are nitriding, DLC coating, and duplex nitriding + DLC coating, and their properties were subsequently characterized.

- The nitriding process modifies the surface and the microstructural characteristics of the tool steels, enhancing wear resistance and surface durability.
- Commercially coated ta-C produces a high-quality DLC coating.
- SEM cross sections confirm a uniform DLC with a thickness of approximately 400 nm.
- The uncoated samples suffer extensive delaminations and oxide formation, resulting in large track widths under 10 N and 20 N loads.
- EDX analyses highlight confined oxidative wear with reduced oxygen peaks at increased loads in treated samples.
- Duplex nitrided and DLC samples provided extremely high reduction in wear tracks compared to the uncoated baseline sample.

Raman and XPS analysis demonstrate that the commercially coated (IonBond) ta-C exhibits high-quality DLC chemistry. The tribological data confirm that single surface treatments are limited under high loads due to the low thickness of the coating. The duplex nitrided and DLC samples provided a high reduction in wear tracks compared to the uncoated and DLC-only samples. Therefore, while ta-C material is of high quality, the duplex strategy is identified as the optimal solution for industrial applications, even under high contact loads. The study presents surface treatment enhancements that align with industrial demands for sustainable, low-friction tooling and can be positioned as an optimal strategy for extending tool life in high-volume cold forming operations.

ACKNOWLEDGMENT

This study was supported by Kastamonu University Scientific Research Projects Coordination Unit (KUBAP) under project number KUBAP-01/2021-23.

REFERENCES

[1] S. Jie, H. Tian, J. Li, P. Zhang, Z. Hong, S. An, Study on the working performance of CrAlCN coated and uncoated carbide twist drill, Optik (Stuttg). 270 (2022) 169948. https://doi.org/10.1016/j.ijleo.2022.169948.

[2] P.A. Primeaux, B. Zhang, W.J. Meng, Performance of micro-drilling of hard Ni alloys using coated and uncoated WC/Co bits, Engineering Research Express 1 (2019) 0–18. https://doi.org/10.1088/2631-8695/ab383e.

[3] N. Mokas, S. Bouadila, A. Amirat, Contradictory effects of machining conditions on wear in the main cutting zones of the twist drill, Journal of the Brazilian Society of Mechanical Sciences and Engineering 45 (2023) 1–15. https://doi.org/10.1007/s40430-023-04459-5.

[4] R. Zhang, Z. Liang, L. Yi, J. Hu, Y. Du, L. Guo, Y. Ma, R. Cai, Q. Zhao, L. Xiong, Research on the design and cutting performance of a novel BTA boring tool intended for machining of nickel-based superalloys, Journal of Materials Research and Technology 36 (2025) 7980–7995. https://doi.org/10.1016/j.jmrt.2025.05.022.

[5] J.E. Field, Natural Diamond: The Standard, in: 1991: pp. 17–35. https://doi.org/10.1007/978-1-4684-5967-8_2.

[6] P.K. Bachmann, R. Messier, Emerging Technology of Diamond Thin Films, Chemical & Engineering News Archive 67 (1989) 24–38. https://doi.org/10.1021/cen-v067n020.p024.

[7] M. Amaral, D.J. Carreira, A.J.S. Fernandes, C.S. Abreu, F.J. Oliveira, J.R. Gomes, R.F. Silva, A DLC/diamond bilayer approach for reducing the initial friction towards a high bearing capacity, Wear 290–291 (2012) 18–24. https://doi.org/10.1016/j.wear.2012.05.026.

[8] X. Meng, K. Zhang, X. Guo, C. Wang, L. Sun, Preparation of micro-textures on cemented carbide substrate surface by plasma-assisted laser machining to enhance the PVD tool coatings adhesion, J. Mater. Process. Technol. 288 (2021) 116870. https://doi.org/10.1016/j.jmatprotec.2020.116870.

[9] T. Katoh, T. Aizawa, T. Yamaguchi, Plasma assisted nitriding for micro-texturing onto martensitic stainless steels ∗, Manuf. Rev. (Les. Ulis). 2 (2015). https://doi.org/10.1051/mfreview/2015004.

[10] V. Kundrát, X. Zhang, K. Cooke, H. Sun, J. Sullivan, H. Ye, A novel Mo-W interlayer approach for CVD diamond deposition on steel, AIP Adv. 5 (2015). https://doi.org/10.1063/1.4918969.

[11] A.M. Grishin, V. V Putrolaynen, Hard and Highly Adhesive AlMgB14 Coatings RF Sputtered on Tungsten Carbide and High-Speed Steel, Materials 16 (2023) 6930. https://doi.org/10.3390/ma16216930.

[12] T. Hao, J. Du, G. Su, P. Zhang, Y. Sun, J. Zhang, Mechanical and cutting performance of cemented carbide tools with Cr/x/DLC composite coatings, International Journal of Advanced Manufacturing Technology 106 (2020) 5241–5254. https://doi.org/10.1007/s00170-020-05014-5.

[13] Z. Zeng, L. Yang, Q. Zeng, H. Lou, H. Sheng, J. Wen, D.J. Miller, Y. Meng, W. Yang, W.L. Mao, H.K. Mao, Synthesis of quenchable amorphous diamond, Nat. Commun. 8 (2017) 322. https://doi.org/10.1038/s41467-017-00395-w.

[14] T.A. Friedmann, J.P. Sullivan, J.A. Knapp, D.R. Tallant, D.M. Follstaedt, D.L. Medlin, P.B. Mirkarimi, Thick stress-free amorphous-tetrahedral carbon films with hardness near that of diamond, Appl. Phys. Lett. 71 (1997) 3820–3822. https://doi.org/10.1063/1.120515.

[15] P.H. Gaskell, A. Saeed, P. Chieux, D.R. McKenzie, The structure of highly tetrahedral amorphous diamond-like carbon: I. Neutron scattering studies, Philosophical Magazine B: Physics of Condensed Matter; Statistical Mechanics, Electronic, Optical and Magnetic Properties 66 (1992) 155–169. https://doi.org/10.1080/13642819208224580.

[16] T. Miyazawa, S. Misawa, S. Yoshida, S.I. Gonda, Preparation and structure of carbon film deposited by a mass-separated C+ ion beam, J. Appl. Phys. 55 (1984) 188–193. https://doi.org/10.1063/1.332862.

[17] B. Rothammer, M. Schwendner, M. Bartz, S. Wartzack, T. Böhm, S. Krauß, B. Merle, S. Schroeder, M. Uhler, J.P. Kretzer, V. Weihnacht, M. Marian, Wear Mechanism of Superhard Tetrahedral Amorphous Carbon (ta-C) Coatings for Biomedical Applications, Adv. Mater. Interfaces 10 (2023). https://doi.org/10.1002/admi.202202370.

[18] A. Götze, S. Makowski, T. Kunze, M. Hübner, H. Zellbeck, V. Weihnacht, A. Leson, E. Beyer, J. Joswig, G. Seifert, G. Abrasonis, M. Posselt, J. Fassbender, W. Möller, S. Gemming, M. Krause, Tetrahedral Amorphous Carbon Coatings for Friction Reduction of the Valve Train in Internal Combustion Engines, Adv. Eng. Mater. 16 (2014) 1226–1233. https://doi.org/10.1002/adem.201400188.

[19] A. Iyer, A. Kaskela, S. Novikov, J. Etula, X. Liu, E.I. Kauppinen, J. Koskinen, Effect of tetrahedral amorphous carbon coating on the resistivity and wear of single-walled carbon nanotube network, J. Appl. Phys. 119 (2016). https://doi.org/10.1063/1.4948672.

[20] N. Wester, J. Etula, T. Lilius, S. Sainio, T. Laurila, J. Koskinen, Selective detection of morphine in the presence of paracetamol with anodically pretreated dual layer Ti/tetrahedral amorphous carbon electrodes, Electrochem. Commun. 86 (2018) 166–170. https://doi.org/10.1016/j.elecom.2017.12.014.

[21] P.A. Romero, L. Pastewka, J. Von Lautz, M. Moseler, Surface passivation and boundary lubrication of self-mated tetrahedral amorphous carbon asperities under extreme tribological conditions, Friction 2 (2014) 193–208. https://doi.org/10.1007/s40544-014-0057-z.

[22] P. Fabisch, V. Voropai, M. Nieher, A. Buchholz, S. Weissmantel, C.H. Lohmann, J. Bertrand, J. Döring, Biocompatibility and Antibacterial Potential of Tetrahedral Amorphous Carbon (ta-C) Coatings on CoCrMo Alloy for Articulating Implant Surfaces, J. Biomed. Mater. Res. A 113 (2025). https://doi.org/10.1002/jbm.a.37815.

[23] S. Sainio, D. Nordlund, M.A. Caro, R. Gandhiraman, J. Koehne, N. Wester, J. Koskinen, M. Meyyappan, T. Laurila, Correlation between sp 3 -to-sp 2 Ratio and Surface Oxygen Functionalities in Tetrahedral Amorphous Carbon (ta-C) Thin Film Electrodes and Implications of Their Electrochemical Properties, The Journal of Physical Chemistry C 120 (2016) 8298–8304. https://doi.org/10.1021/acs.jpcc.6b02342.

[24] J. Wei, P. Guo, L. Liu, H. Li, H. Li, S. Wang, P. Ke, H. Saito, A. Wang, Corrosion resistance of amorphous carbon film in 3.5 wt% NaCl solution for marine application, Electrochim. Acta 346 (2020). https://doi.org/10.1016/j.electacta.2020.136282.

[25] M. Muhammed, M. Javidani, T. Ebrahimi Sadrabadi, M. Heidari, T. Levasseur, M. Jahazi, A Comprehensive Review of Cathodic Arc Evaporation Physical Vapour Deposition (CAE-PVD) Coatings for Enhanced Tribological Performance, Coatings 14 (2024). https://doi.org/10.3390/coatings14030246.

[26] I.P. Filos, R. Sesana, M. Di Biase, R. Lupoi, New abrasive coatings: Abraded volume measurements in ceramic ball production, Journal of Manufacturing and Materials Processing 5 (2021). https://doi.org/10.3390/jmmp5030081.

[27] S. Sharma, S. Sangal, K. Mondal, On the optical microscopic method for the determination of ball-on-flat surface linearly reciprocating sliding wear volume, Wear 300 (2013) 82–89. https://doi.org/10.1016/j.wear.2013.01.107.

[28] P. Pawlus, R. Reizer, Accurate determination of wear volume of ball employed as counter sample in reciprocating sliding tests, Wear 580–581 (2025) 206309. https://doi.org/10.1016/j.wear.2025.206309.

[29] A.C. Ferrari, J. Robertson, Interpretation of Raman spectra of disordered and amorphous carbon, Phys. Rev. B 61 (2000) 14095–14107. https://doi.org/10.1103/PhysRevB.61.14095.

[30] A.C. Ferrari, J. Robertson, Resonant Raman spectroscopy of disordered, amorphous, and diamondlike carbon, Phys. Rev. B Condens. Matter Mater. Phys. 64 (2001) 1–13. https://doi.org/10.1103/PhysRevB.64.075414.

[31] C. Casiraghi, A.C. Ferrari, J. Robertson, Raman spectroscopy of hydrogenated amorphous carbons, Phys. Rev. B Condens. Matter Mater. Phys. 72 (2005) 1–14. https://doi.org/10.1103/PhysRevB.72.085401.

[32] F. Alvarez-Antolin, A. Gonzalez-Pociño, A. Cofiño-Villar, C.H. Alvarez-Perez, Optimisation of Thermal Processes with Plasma Nitriding on Vanadis 4 High Speed Steel, Materials 15 (2022) 906. https://doi.org/10.3390/ma15030906.
[33] E.A. dos Santos de Almeida, J.C.G. Milan, C.E. da Costa, C. Binder, J.D.B. de Mello, H.L. Costa, Combined Use of Surface Texturing, Plasma Nitriding and DLC Coating on Tool Steel, Coatings 11 (2021) 201. https://doi.org/10.3390/coatings11020201.
[34] I. Gómez, J.A. García, J.A. Santiago, I. Fernandez, P. Jose Fernandez, I. Braceras, Adhesion Enhancement on a Duplex DLC HiPIMS Positive Pulse Coating Performed by Active Screen Plasma Nitriding Pretreatment on 316L Stainless Steel Substrate, Advances in Materials Science and Engineering 2022 (2022) 1–11. https://doi.org/10.1155/2022/5621154.
[35] A. Mannan, M.F.M. Sabri, Md.A. Kalam, H.H. Masjuki, Tribological Properties of Steel/Steel, Steel/DLC and DLC/DLC Contacts in the Presence of Biodegradable Oil, Journal of the Japan Petroleum Institute 62 (2019) 11–18. https://doi.org/10.1627/jpi.62.11.
[36] T.F. Zhang, K.-W. Kim, K.H. Kim, Nitrogen-Incorporated Hydrogenated Amorphous Carbon Film Electrodes on Ti Substrates by Hybrid Deposition Technique and Annealing, J. Electrochem. Soc. 163 (2016) E54–E61. https://doi.org/10.1149/2.0051603jes.
[37] X. Chen, X. Wang, D. Fang, A review on C1s XPS-spectra for some kinds of carbon materials, Fullerenes Nanotubes and Carbon Nanostructures 0 (2020) 1048–1058. https://doi.org/10.1080/1536383X.2020.1794851.
[38] S. Bhattacharyya, J. Hong, G. Turban, Determination of the structure of amorphous nitrogenated carbon films by combined Raman and x-ray photoemission spectroscopy, J. Appl. Phys. 83 (1998) 3917–3919. https://doi.org/10.1063/1.367312.
[39] J. Zhu, B. Liu, L. Li, Z. Zeng, W. Zhao, G. Wang, X. Guan, Simple and Green Fabrication of a Superhydrophobic Surface by One-Step Immersion for Continuous Oil/Water Separation, J. Phys. Chem. A 120 (2016) 5617–5623. https://doi.org/10.1021/acs.jpca.6b06146.
[40] K. Yamamoto, Chemical bond analysis of amorphous carbon films, Vacuum 84 (2009) 638–641. https://doi.org/10.1016/j.vacuum.2009.10.016.
[41] M. Kano, J.M. Martin, M.I. De Barros Bouchet, Green Superlubrication by Hydrogen-Free Amorphous Carbon with Human Friendly Lubricants, Sensors and Materials (2017) 771. https://doi.org/10.18494/SAM.2017.1630.
[42] E.C.T. Ba, P.S. Martins, M.B. da Silva, A.J. dos Santos, M.R. Dumont, P.M. Firpe, G.F.S. de Melo Nogueira, P.A.A. Magalhães Júnior, Study of the structural and tribological characteristics of hydrogenated diamond-like carbon coatings for high-speed steel substrate applications, Tribol. Int. 212 (2025). https://doi.org/10.1016/j.triboint.2025.110941.
[43] S.N. Grigoriev, M.A. Volosova, S. V. Fedorov, M. Mosyanov, Influence of DLC Coatings Deposited by PECVD Technology on the Wear Resistance of Carbide End Mills and Surface Roughness of AlCuMg2 and 41Cr4 Workpieces, Coatings 10 (2020) 1038. https://doi.org/10.3390/coatings10111038.
[44] J. Decrozant-Triquenaux, L. Pelcastre, C. Courbon, B. Prakash, J. Hardell, High temperature tribological behaviour of PVD coated tool steel and aluminium under dry and lubricated conditions, Friction 9 (2021) 802–821. https://doi.org/10.1007/s40544-020-0435-7.
[45] L. Chagas da Silva, M.S. Libório, P.A. Radi, D.A. Pereira Reis, V.J. Trava-Airoldi, T.F. da Conceição Hermenegildo, S.M. Alves, DLC/a-Si:H multilayers films to improve wear resistance of components of common rail injection system, Journal of Materials Research and Technology 26 (2023) 2617–2628. https://doi.org/10.1016/j.jmrt.2023.08.078.
[46] A. Claver, E. Jiménez-Piqué, J.F. Palacio, E. Almandoz, J. Fernández de Ara, I. Fernández, J.A. Santiago, E. Barba, J.A. García, Comparative Study of Tribomechanical Properties of HiPIMS with Positive Pulses DLC Coatings on Different Tools Steels, Coatings 11 (2020) 28. https://doi.org/10.3390/coatings11010028.
[47] H. Paschke, M. Weber, P. Kaestner, G. Braeuer, Influence of different plasma nitriding treatments on the wear and crack behavior of forging tools evaluated by Rockwell indentation and scratch tests, Surf. Coat. Technol. 205 (2010) 1465–1469. https://doi.org/10.1016/j.surfcoat.2010.07.053.
[48] C. Zhao, C.X. Li, H. Dong, T. Bell, Study on the active screen plasma nitriding and its nitriding mechanism, Surf. Coat. Technol. 201 (2006) 2320–2325. https://doi.org/10.1016/j.surfcoat.2006.03.045.
[49] A.K. Gonzalez-Moran, M. Naeem, H.M. Hdz-García, E.E. Granda-Gutiérrez, J.J. Ruíz-Mondragón, M. Alvarez-Vera, J.C. Díaz-Guillén, Improved mechanical and wear properties of H13 tool steel by nitrogen-expanded martensite using current-controlled plasma nitriding, Journal of Materials Research and Technology 25 (2023) 4139–4153. https://doi.org/10.1016/j.jmrt.2023.06.221.
[50] O. Kubaschewski, C.B. Alcock, Metallurgical Thermochemistry, Pergamon Press, 1979. https://onlinelibrary.wiley.com/doi/10.1002/crat.19800150208.
[51] E.J. Mittemeijer, Fundamentals of Nitriding and Nitrocarburizing, in: Steel Heat Treating Fundamentals and Processes, ASM International, 2013: pp. 619–646. https://doi.org/10.31399/asm.hb.v04a.a0005818.